## Propagating wave merging in a precipitation reaction **⊘**

Boshir Ahmed <sup>®</sup> ; David Mersing <sup>®</sup> ; Mark R. Tinsley ■ <sup>®</sup> ; Kenneth Showalter <sup>®</sup>



Chaos 33, 043105 (2023)

https://doi.org/10.1063/5.0139698





CrossMark





## Propagating wave merging in a precipitation reaction

Cite as: Chaos 33, 043105 (2023); doi: 10.1063/5.0139698 Submitted: 22 December 2022 · Accepted: 13 March 2023 · Published Online: 3 April 2023







Boshir Ahmed,<sup>a)</sup> David Mersing,<sup>b)</sup> Mark R. Tinsley,<sup>c)</sup> Dand Kenneth Showalter<sup>d)</sup> David Mersing,<sup>b)</sup>





## **AFFILIATIONS**

C. Eugene Bennett Department of Chemistry, West Virginia University, Morgantown, West Virginia 26506-6045, USA

- <sup>a)</sup>Electronic address: ma0237@mix.wvu.edu
- b) Electronic address: damersing@mix.wvu.edu
- c)Author to whom correspondence should be addressed: mark.tinsley@mail.wvu.edu
- d) Electronic address: kshowalt@wvu.edu

#### **ABSTRACT**

Propagating precipitation waves are a remarkable form of spatiotemporal behavior that arise through the coupling of reaction, diffusion, and precipitation. We study a system with a sodium hydroxide outer electrolyte and an aluminum hydroxide inner electrolyte. In a redissolution Liesegang system, a single propagating precipitation band moves down through the gel, with precipitate formed at the band front and precipitate dissolved at the band back. Complex spatiotemporal waves occur within the propagating precipitation band, including counter-rotating spiral waves, target patterns, and annihilation of waves on collision. We have also carried out experiments in thin slices of gel, which have revealed propagating waves of a diagonal precipitation feature within the primary precipitation band. These waves display a wave merging phenomenon in which two horizontally propagating waves merge into a single wave. Computational modeling permits the development of a detailed understanding of the complex dynamical behavior.

Published under an exclusive license by AIP Publishing. https://doi.org/10.1063/5.0139698

Stationary precipitation patterns formed via the coupling of reaction, diffusion, and precipitation were originally reported by Liesegang in 1896. Propagating precipitation patterns were first observed more recently.<sup>2-5</sup> These propagating waves involve both solid and solution phases and, though intrinsically three-dimensional in nature, have many characteristics of two-dimensional solution phase reaction-diffusion waves.<sup>2,3,6</sup> The similarities between the two types of behavior are also remarkable in that, in contrast to other reaction-diffusion waves, precipitation wave propagation does not involve an autocatalytic species.<sup>6,7</sup> It can be understood in terms of the coupling of templated growth to changes in permeability due to the temporary formation of a semi-permeable membrane. 3,4,8 These features offer potential applications for ion-selection and microstructure fabrication.9 In this work, we focus on a redissolution Liesegang system that demonstrates anomalous dispersion, in which a trailing wave is capable of catching up and annihilating with the wave immediately ahead of it. 10 We present a mechanistic understanding of this behavior based upon feedback through critical concentration gradients.

#### I. INTRODUCTION

A Liesagang system involves the diffusion of an outer electrolyte into a region containing an inner electrolyte with which it is capable of forming a precipitate. 1,11-14 The inner electrolyte is normally contained within a porous gel that prevents convective motion of the liquids. The outer electrolyte concentration is typically significantly larger than the inner electrolyte concentration. As the outer electrolyte diffuses through the gel, these systems can display a number of interesting spatiotemporal behaviors including periodic precipitation patterns.9,15,16

A redissolution Liesegang system is one in which excess of the outer electrolyte forms a soluble complex with the original precipitation species.<sup>5</sup> Two types of behavior are typical in such systems. The first is a set of pseudo-traveling precipitation bands.<sup>5,17</sup> Precipitation bands form at the diffusive front with the same regularity as with the normal Liesegang system. However, in the redissolution system, the earlier bands slowly dissolve due to the increasing outer electrolyte concentration. The resulting effect is an apparent traveling set of bands moving down through the gel. However, each band is actually static with new bands being formed at the front and old bands dissolving at the back.

The second behavior seen in redissolution Liesegang systems involves the propagation of a single traveling precipitation band that moves down through the gel.<sup>17,18</sup> New precipitate is continuously formed at the front of the band and continuously dissolves at the back of the band. A number of studies have identified a remarkable secondary phenomenon that can occur in this latter system involving complex spatiotemporal waves that occur within the propagating precipitation band. 2,3,19,20 When viewed from above, these patterns can appear similar to the spiral waves observed in thin films of Belousov–Zhabotinsky (BZ) solution.<sup>6,7</sup> At other concentrations, the behavior is more akin to spatiotemporal chaos.<sup>21</sup> Experiments using thin slices of gel have shown that these patterns involve waves composed of a moving diagonal precipitation feature within the main precipitation band, which is traveling down through the gel.<sup>2,3</sup> This demonstrates that the waves are three-dimensional in nature, with the top-view experiments offering a 2D perspective on the behavior.19,3

In this work, we will focus on a redissolution system in which the secondary wave behavior involves the amphoteric properties of  $Al(OH)_3$ . This insoluble hydroxide first forms as a precipitate and then dissolves through the formation of the soluble complex ion  $Al(OH)_4^-$  in excess hydroxide,<sup>2</sup>

$$Al^{3+}(aq) + 3OH^{-}(aq) \rightarrow Al(OH)_{3}(s),$$
  
 $Al(OH)_{3}(s) + OH^{-}(aq) \rightarrow Al(OH)_{4}(aq).$ 

In particular, we will explore the unusual behavior that under appropriate conditions a wave can catch up with the wave immediately ahead of it. The two waves then merge to form a single wave. This type of behavior has previously been seen in excitation systems that have anomalous dispersion relationships. 10,22-25 In a general excitation wave system, the dependence of the velocity of a wave with its distance from the previous wave is given by the system's dispersion relationship. For a system with a normal dispersion relationship, the wave velocity decreases as this separation decreases, and hence, a trailing wave will not catch up with a lead wave. This occurs because the presence of the decaying inhibitor from the previous excitation wave slows the buildup of autocatalyst associated with the next wave. The smaller the separation of the waves, the more inhibitor a trailing wave experiences and, therefore, the slower its velocity. 10

In the case of anomalous dispersion, the velocity of the trailing wave can increase as the separation decreases, giving the appearance that there is an attraction between two successive waves. This can result in wave stacking and/or merging of a trailing wave with a lead wave. <sup>10,24</sup> Anomalous dispersion has previously been reported in the mercuric iodide precipitation system. <sup>20</sup>

#### **II. METHODS**

## A. Gel preparation

Gels are prepared in a similar manner to preparations used in previous studies.<sup>3</sup> An agarose gel is prepared by dissolving 1.0 g

of agarose powder in 100.0 ml of de-ionized water. The solution is heated and stirred until it reaches 90 °C. The solution is removed from the heat source and stirred for an additional 10 min. Powdered aluminum chloride hexahydrate,  $AlCl_3 \cdot 6H_2O$ , is added to this solution and stirred until the salt is completely dissolved. The liquid gel is then transferred to the appropriate container, depending on the experimental setup.

#### **B.** Experimental configurations

Two different experimental configurations are used in this study: a gel disk configuration and a gel slice configuration, Fig. 1. In the gel disk configuration, 30.0 ml of the AlCl<sub>3</sub> liquid gel is poured into a Petri dish (45 mm radius) and allowed to solidify at room temperature. The Petri dish containing the gel disk is placed on top of a Kaiser Slimlite Plano LED array and then 30.0 ml of a 2.5M sodium hydroxide solution is poured on top of the gel disk. The reaction is monitored using a charged-coupled device (CCD) camera positioned above the gel. Images of the gel disk are taken every 2 s by the CCD camera for the duration of an experiment.

In the gel slice experiments,  $5.0\,\mathrm{ml}$  of the AlCl<sub>3</sub> liquid gel is poured between two glass microscope slides ( $50\times75\,\mathrm{mm^2}$ ) that are separated by  $1.0\,\mathrm{mm}$  thick Teflon spacers. The slides are clamped together to prevent leakage. The liquid gel solution is allowed to solidify at room temperature. The gel slab is placed in front of a white background and is illuminated from the front by a Bridgelux  $10000\mathrm{LM}$  LED array. Next,  $3.5\,\mathrm{ml}$  of a  $2.5\mathrm{M}$  NaOH solution is added to the top of the gel slap. During some experiments, bromothymol blue pH indicator is added to both the gel and NaOH solutions. A CCD camera device records images of the reaction every  $2\,\mathrm{s}$ .

## **III. EXPERIMENTAL OBSERVATIONS**

Wave phenomena in the system vary depending on both the inner and outer electrolyte concentrations. For a fixed outer electrolyte concentration, within the range used in our experiments, the wave activity is typically sparse at low [Al3+], with a physical perturbation required to start a wave. As the [Al3+] is increased, the number of spontaneous centers of wave activity increases.<sup>2,4</sup> These spontaneous centers initially consist of a pair of nearby meandering counter-rotating spiral tips, which produce a target-like propagating wave pattern. An example image from a gel disk experiment is shown in Fig. 1(a). Figure 1(b) shows an example of wave behavior seen using a gel slice experiment. This perspective demonstrates that the wave propagation is associated with a diagonal precipitation feature moving within the precipitation band. This feature is composed of a wave tip, a wave middle, and a wave back. Previous studies indicate that the wave back corresponds to the front of the white region of a wave seen in the gel disk experiments.3 Therefore, the wave back is the region that has the highest transparency to light.

Studies have further indicated that the precipitate that composes the precipitation band and the precipitate that composes the diagonal feature have different physico-chemical properties.<sup>3</sup> It is convenient to designate the two precipitates as  $P_1$  and  $P_2$ , respectively. The wave tip occurs close to the leading edge of the

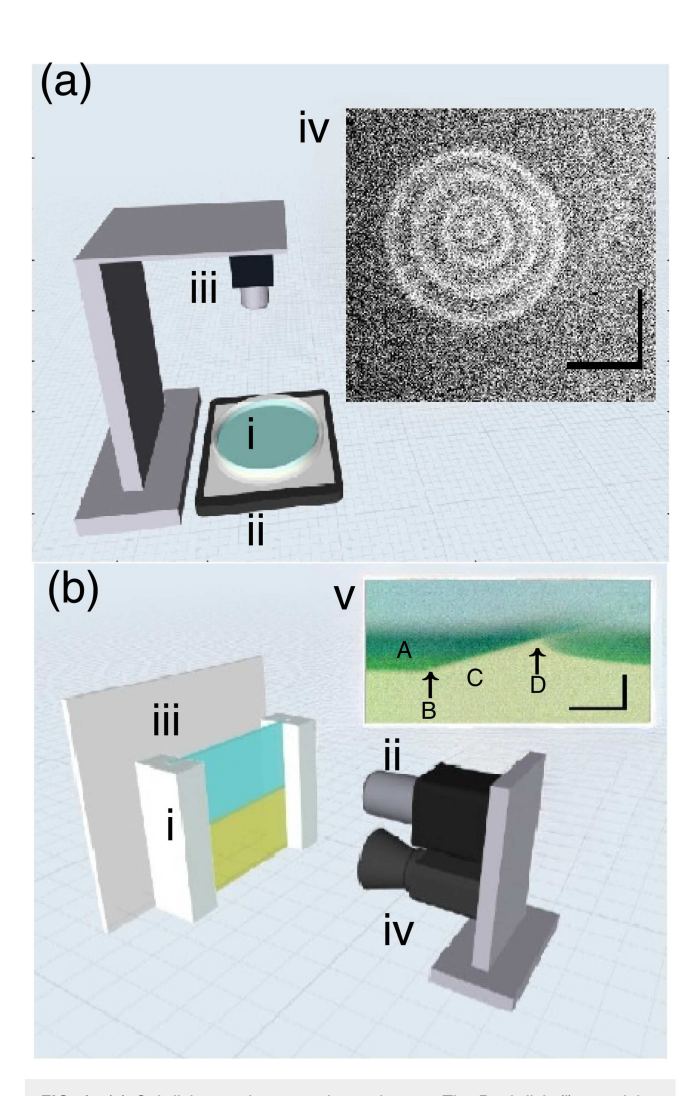


FIG. 1. (a) Gel disk, top-view, experimental setup. The Petri dish (i) containing the AlCl<sub>3</sub>/gel and NaOH is placed on top of a LED array (ii). The reaction is monitored by a CCD camera (iii) recording images every 2 s. (iv) Typical experimental image taken using this setup showing a target-like series of waves propagating from a pair of counter-rotating spirals. (b) Gel slice, side-view, experimental setup. The reactor consists of a pair of microscope slides (i) containing the AlCl<sub>3</sub>/gel and NaOH solution placed between a CCD camera (ii) and a white background (iii). The reactor is illuminated by a light source (iv) and images are recorded every 2 s. (v) Typical experimental image showing a precipitation band and a propagating wave structure traveling from right to left. In this experimental image, the indicator bromothymol blue has been added to the system. (a) Precipitation band, (b) wave tip, which is the leading edge of the diagonal precipitation feature, and (c) wave middle, (d) wave back, which is the location where the precipitation band reattaches to the diagonal precipitation feature. 1 mm scale bars are shown in each image.

horizontal precipitation band and is the location of new  $P_2$  precipitation growth. The wave middle is a solid line of precipitate below which no precipitation band is observed. The color of the indicator (blue/green: basic, yellow: acidic), Fig. 1(b), on either side of the

wave middle indicates that the precipitate in this region does not allow the passage of hydroxide ions.  $^{8,27}$  The wave back is located where the line of diagonal  $P_2$  precipitate rapidly thins and the main  $P_1$  precipitation band reforms.

Further increases in  $[Al^{3+}]$  lead to an increasing number of spontaneously formed centers and the onset of unstable spatiotemporal patterns. At higher  $[Al^{3+}]$  concentration, the wave behavior becomes extremely complex and shows characteristics of spatiotemporal chaos.<sup>21</sup>

Wave merging is best discernible at lower [Al³+] where fewer spontaneous centers are present. Figure 2 shows a series of target-like waves that originate from such a center. Typically, in such an experiment, the even numbered waves catch up and merge with the odd numbered waves. In a given experiment, this usually occurs for the first three or four pairs of waves. Wave merging of the first pair of waves can be seen in Fig. 2 where the second wave catches up with the first wave. The fourth wave can be seen catching up with the third wave in Figs. 2(b)–2(f). From this top-view perspective, each trailing, even numbered wave appears to merge with its corresponding leading, odd numbered wave, resulting in a single remaining wave in each case.

The gel slice experiments, Fig. 3, reveal different details of the wave behavior. We see a wave train of four waves traveling from left to right. Here, we initially focus on two of the waves, which for convenience are labeled 1 and 2. Their behaviors correspond to those of a lead wave and merging trailing wave, respectively. By observation of the thin trail of  $P_2$  left by each wave, which acts a tracer of the wave's trajectory, the angle of propagation of the trailing wave is seen to become increasingly shallow as it gets closer to the lead wave. It then runs into the lead wave, close to the lead wave's wave back, and is annihilated leaving only the lead wave propagating forwards, Fig. 3(f). Hence, the process of merging is actually an annihilation process involving the collision of a trailing wave into the back of a lead wave. The trajectories of the wave tips of the two waves are shown in the inset of Fig. 3(f).

The angles of propagation of waves 1, 2, and 3, from Fig. 3, are shown in Fig. 4(a). Wave 1 maintains an approximately constant angle of propagation as it travels down the gel. In contrast, the angle of wave 2 continuously decreases as it approaches annihilation with wave 1. Figure 4(b) shows the horizontal separation of the wave tips of waves 1 and 2. The continuing decrease in their separation indicates that the second wave has a larger wave tip horizontal velocity allowing it to gain on the lead wave. This combined with the decreasing angle of propagation will necessarily result in wave 2 colliding with wave 1. The actual collision itself can be tracked using the horizontal separation of the tip of wave 2 and the wave back of wave 1, Fig. 4(b).

An additional feature of the merging behavior is that as the trailing wave approaches the lead wave, the horizontal length of their wave middles change, Fig. 4(b). (Hereafter, we will refer to the horizontal length of the wave middle as the wavelength. This should not be confused with the standard wavelength, which in this system would refer to the separation of successive wave tips or wave backs.) In the case of the lead wave, the wavelength increases. This is, in part, due to a phenomenon that we have also observed in other experiments that don't display wave merging; the wavelength of a wave increases with time. A secondary component is that the wavelength

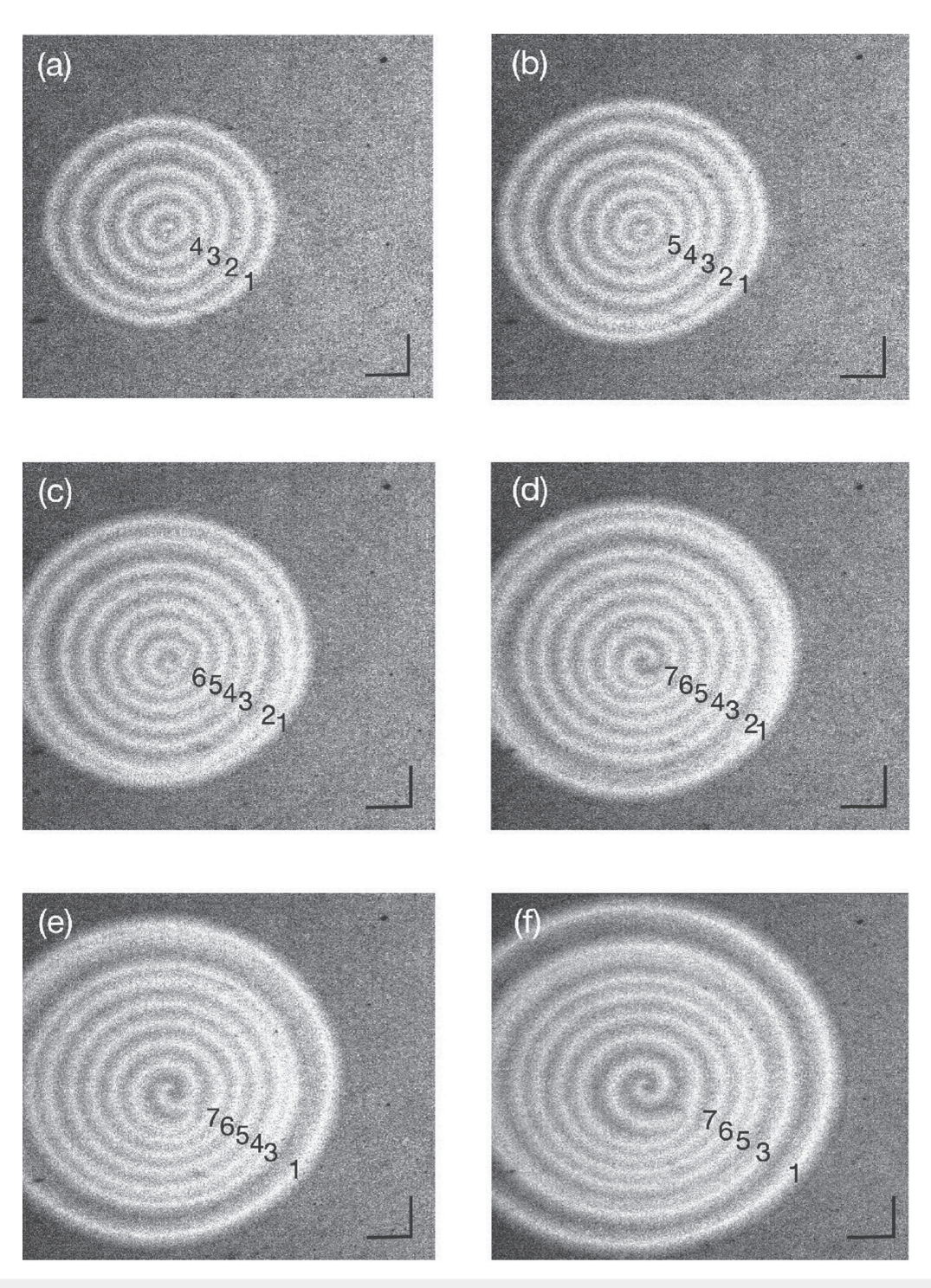


FIG. 2. Sequence of experimental images, taken using the top-view experimental configuration, showing wave merging. The second wave, wave 2, generated by the counter-rotating spiral tips catches up with the first wave, wave 1, and then merges, panel (e). Merging is also seen between waves 3 and 4, panel (f). Images are taken at times 80, 100, 120, 140, 160, and 200 s, (a)–(f), respectively. Experimental conditions: Gel is composed of 1.0% agarose with 0.32M AlCl<sub>3</sub> as the inner electrolyte and 2.5M NaOH as the outer electrolyte. The black scale bars correspond to 1 mm. See supplementary material for the associated video (Multimedia view). Multimedia view: https://doi.org/10.1063/5.0139698.1

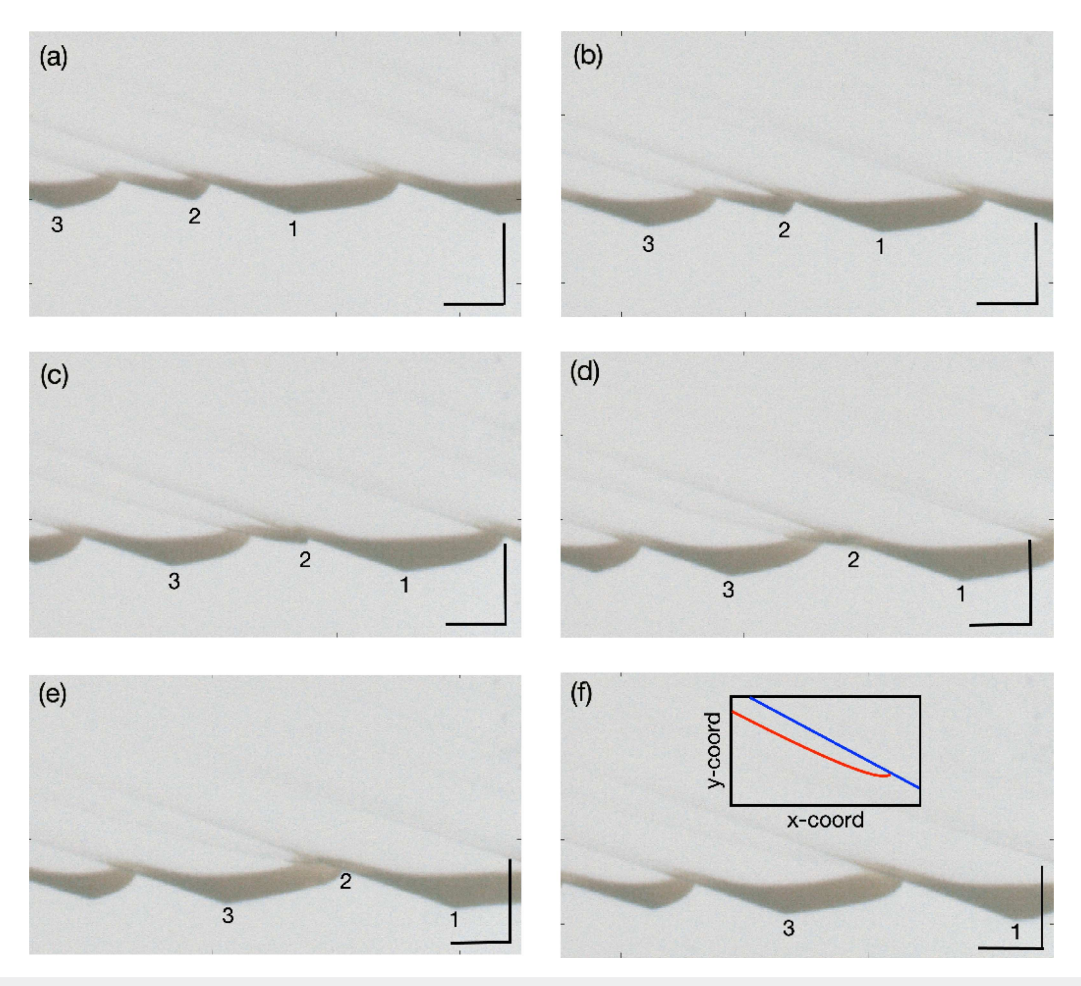


FIG. 3. Sequence of experimental images, taken using the side-view experimental configuration, showing wave merging. The second wave, wave 2, catches up with the first wave, wave 1, and then merges, panels (e) and (f). Images taken at times t = 700, 800, 900, 950, 1000, and 1050 s, (a)–(f), respectively. Inset, subplot (f): Trajectory of wave tips for wave 1, blue, and wave 2, red, between 300 and 1100 s. See Fig. 2 for experimental conditions. The black scale bars correspond to 0.5 mm. See supplementary material for the associated video (Multimedia view). Multimedia view: https://doi.org/10.1063/5.0139698.2

of the lead wave undergoes additional lengthening just prior to the collison of the wave tip.

In contrast, the wavelength of the trailing wave decreases. Since in the gel disk experiments the front of a white region corresponds to a wave back, these changes in wavelengths will appear as the white region of the trailing wave accelerating toward the lead wave. It is the relative changes in these wavelengths combined with the collision of the trailing wave's wave tip with the wave back of the lead wave that corresponds to the wave merging seen from above. Figure 4(b) also shows the separation of wave back 2 and wave back 1. This decreases rapidly as the tip of the trailing wave approaches the wave back of the lead wave.

The angle of propagation of the lead wave is not impacted by the annihilation of the trailing wave. This is reasonable since growth occurs at the wave tip, whereas the collision occurs at the back of the wave. The behavior of wave 3 is virtually identical to wave 1 with a similar angle of propagation and horizontal velocity.

## IV. MODEL DESCRIPTION

We can use simulations of the precipitation system to explore the wave merging phenomenon. The model has been described in full elsewhere. Here, we briefly review. The model assumes that the solid phase is composed of two forms of  $Al(OH)_3$  precipitate,  $P_1$  and  $P_2$ . The former is associated with the band that propagates vertically down the gel. The latter is associated with the wave structure that propagates within the band. Both  $P_1$  and  $P_2$  form via a diffusive intermediate (sol) C. In the case of  $P_1$ , this is represented as

$$A + B \rightarrow C$$
, (1)

$$C \to P_1,$$
 (2)

where A and B are the inner and outer electrolytes, respectively. The rates of these processes are given as  $k_1ab$ ,  $k_2(c-c^*)H(c-c^*)H(p_{2,perm}-p_2)$ , i.e.,  $P_1$  only starts to form if [C] is

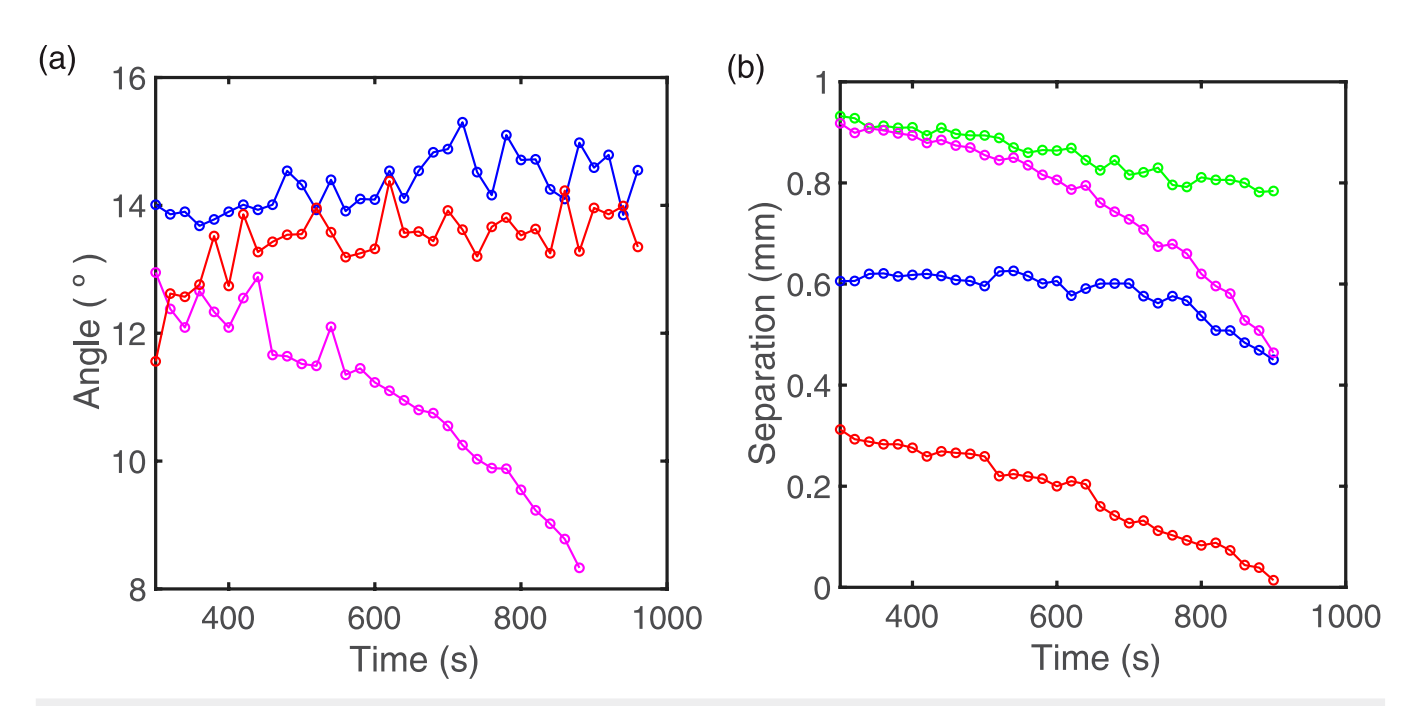


FIG. 4. (a) Angle of depression of wave propagation for waves 1, 2, and 3, blue, magenta, and red, respectively, from Fig. 3. (b) Green line: horizontal separation of wave tip 2 and wave tip 1. Red line: horizontal separation of wave tip 2 and wave back 1. Blue line: wavelength of wave 2. Magenta line: horizontal separation of wave back 2 and wave back 1. Measurements of the locations of wave backs 1 and 2 and wave tip 2 are not possible for a period after 900 s as their positions are not clearly defined, Fig. 3(d). A single well defined wave is again visible at approximately t = 1000 s. Both waves 1 and waves 3 are considered lead waves since they both propagate at an approximately constant angle.

above a critical threshold  $c^*$ . The step function H(s) is defined as H(s) = 1 for s > 0 and H(s) = 0 for  $s \le 0$ . Both  $P_1$  and C can react with excess outer electrolyte B to form inert soluble products (not shown),

$$C + B \rightarrow$$
, (3)

$$P_1 + B \rightarrow$$
, (4)

with rates  $k_3cb$ , and  $k_4p_1b$ , respectively. The latter reaction corresponds to the redissolution of the precipitate  $P_1$ .

Precipitate  $P_2$  is likewise formed directly from C and undergoes redissolution through reaction with excess B, to form inert soluble products, with rates  $k_5(c-c^{**})H(c-c^{**})H(p_2^*-p_2)$  and  $k_6p_2b$ , respectively.

$$C \to P_2,$$
 (5)

$$P_2 + B \rightarrow .$$
 (6)

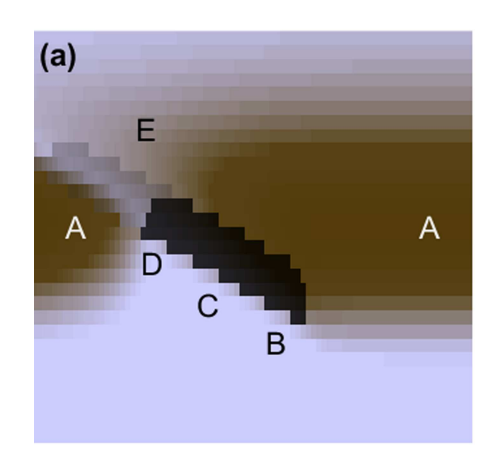
Again [C] has to be above a critical amount  $c^{**}$  for growth of the precipitate to occur. Further to this, growth is only allowed if there is  $P_2$  present in a cell or if  $p_2 \geq p_2^*$  in a spatially adjacent cell. We refer to this initiation of growth of  $P_2$  in a neighboring cell as a templating process, and it results in the formation of a spatially contiguous structure of  $P_2$  in the simulation. This  $P_2$  structure has three characteristic features, the wave tip, the wave middle, and the wave back, see Figs. 1(b) and 5(a).

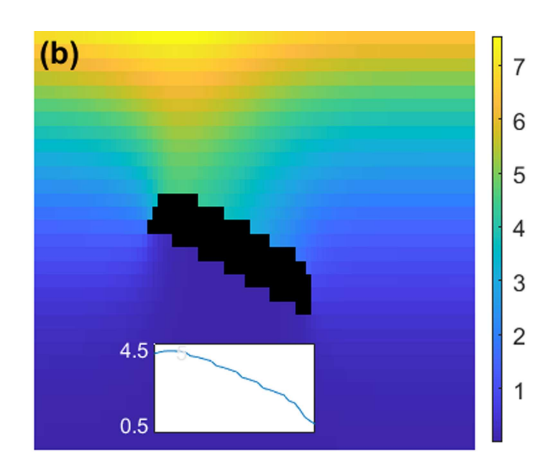
Experimental studies have shown that diffusive transport of both outer and inner electrolytes is not allowed across the wave middle and diffusion recommences at the wave back, Fig. 1(b). This is simulated by not allowing the diffusion of A into or out of a region containing an amount of  $P_2$  above a threshold value,  $p_{2,perm}$ . Species B is likewise not allowed to diffuse out of this region. However, it is allowed to diffuse into the  $P_2$  region, resulting in the slow redissolution of  $P_2$ . Once  $P_2$  drops below the threshold value, normal diffusion of both species reoccurs and the band of  $P_1$  reforms at the tail of the fading  $P_2$  structure. We refer to this region as the wave back.

Further details of the model including boundary and initial conditions are given in the supplementary material.

## V. PRECIPITATION BAND (P1) PROPAGATION

The main precipitation band seen in the experimental system consists of the precipitate  $P_1$ . Its formation can be understood using our simulation, Fig. 5, through the diffusion and reaction of the outer and inner electrolytes. In regions where they are both substantially present, these species react with each other leading to a buildup in C. Once C is above a critical threshold,  $P_1$  starts to form. This defines the sharp leading edge of the precipitation band. Increasing the initial outer electrolyte concentration creates a larger diffusion gradient and leads to a faster movement of B through the gel. Ultimately, this increases the precipitation band's (vertical) velocity.





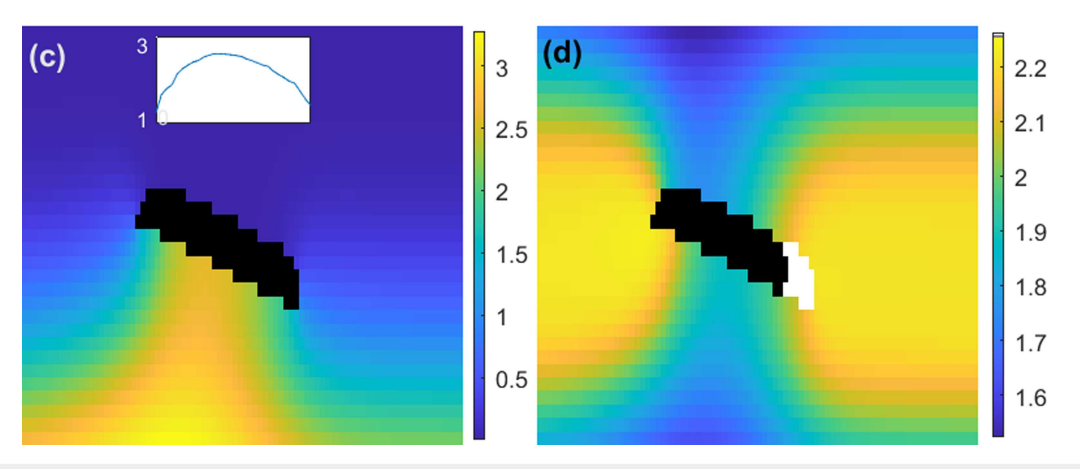


**FIG. 5.** Species distributions near the  $P_2$  diagonal structure. (a)  $P_2$  structure embedded within the precipitation band composed of  $P_1$  (brown). Cells with  $0 < p_2 < p_{2,perm}$  shown in gray. (a) Precipitation band, (b) wave tip, (c) wave middle, (d) wave back, and (e) wave tail. (b) Outer electrolyte concentration. Inset: concentration of outer electrolyte along the region immediately adjacent to the upper perimeter of the  $P_2$  region. (c) Inner electrolyte concentration. Inset: concentration of inner electrolyte along the region immediately adjacent to the lower perimeter of the  $P_2$  region. (d) Sol concentration. The wave tip, shown in white, is defined as the region for which  $dp_2/dt > 0$  and/or  $p_2 > p_2^*$ . (a)—(d) With the exception of the white tip, regions with  $p_2 \ge p_{2,prem}^*$  are shown in black.

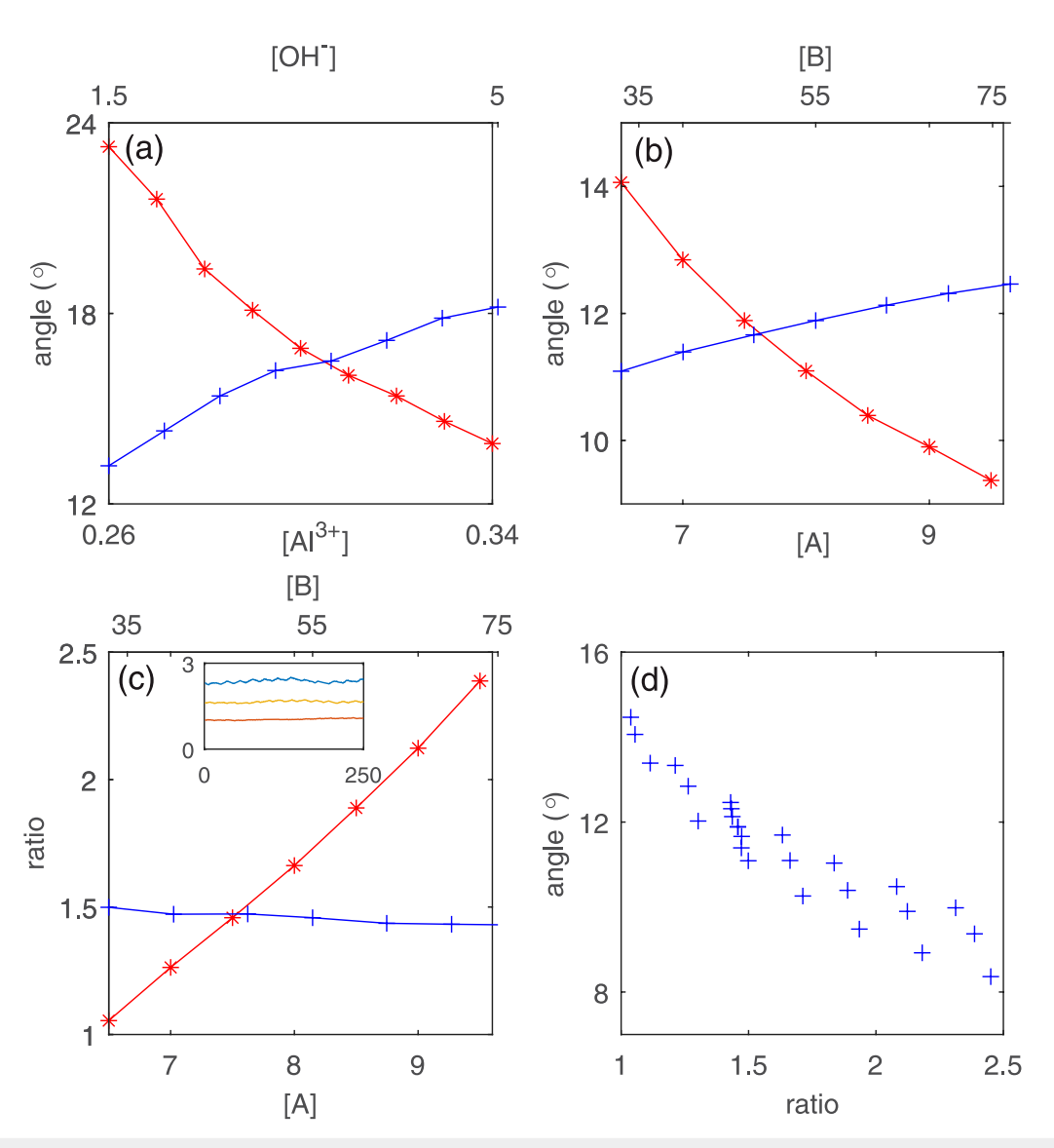
In contrast, increasing the initial inner electrolyte concentration decreases the band's velocity, as the locally excess *A* consumes more *B*, slowing its diffusive intrusion.

## VI. WAVE (P2) PROPAGATION

In the experimental system, the  $P_2$  wave propagates as a diagonal structure that grows at its lower end and dissolves at its upper end. As shown in Fig. 1(b), this structure consists of a wave tip, a wave middle, and a wave back. The equivalent feature seen in the simulations is shown in Fig. 5(a). Essential toward the understanding of the formation and propagation of this  $P_2$  wave is that the structure itself alters the spatial distributions of inner and outer electrolytes in its vicinity. The concentration of the outer electrolyte is relatively high above, Fig. 5(b), and the concentration of the inner

electrolyte is relatively high below, Fig. 5(c), the  $P_2$  feature since neither can diffuse across this region.

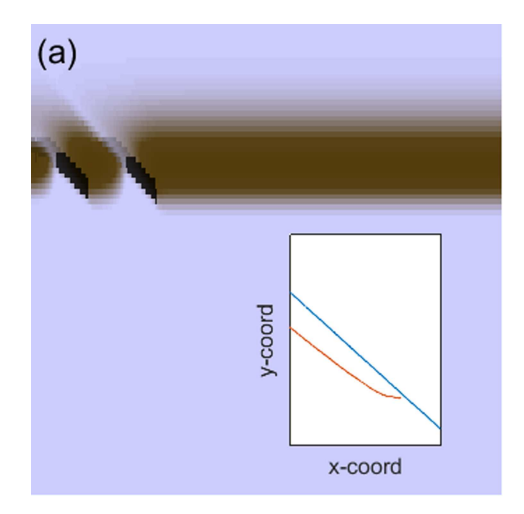
We can understand the direction of  $P_2$  growth by considering a diagonal structure that has already started to develop. As in the case of  $P_1$  formation, the sol must be above a certain value for  $P_2$  to form in a new region. However, in this case,  $P_2$  can only template into an empty region immediately adjacent to a cell when  $[P_2]$  itself is above a certain value,  $p_2^*$ . Hence,  $P_2$  propagation is time sensitive relying upon the simultaneous alignment of the conditions that  $[P_2]$  and [C] are above critical values in contiguous regions. In all parts of the structure, other than the wave tip, sufficient outer electrolyte is present so that  $P_2$  is decreasing (and below the critical threshold). This part of the structure cannot act as a source of new  $P_2$  growth. However, within the vicinity of the wave tip, the outer electrolyte is sufficiently low that  $P_2$  is still in the growth stage.

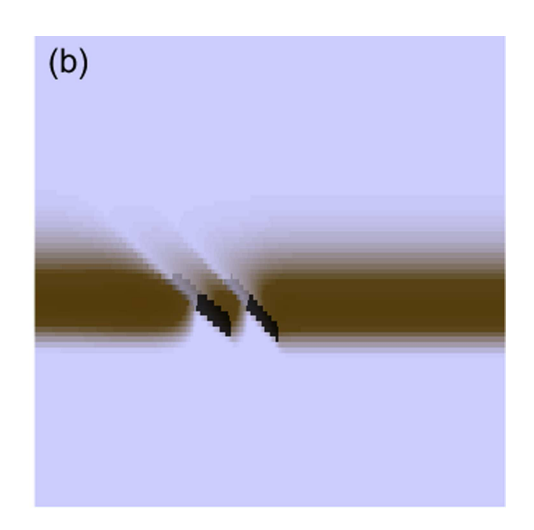


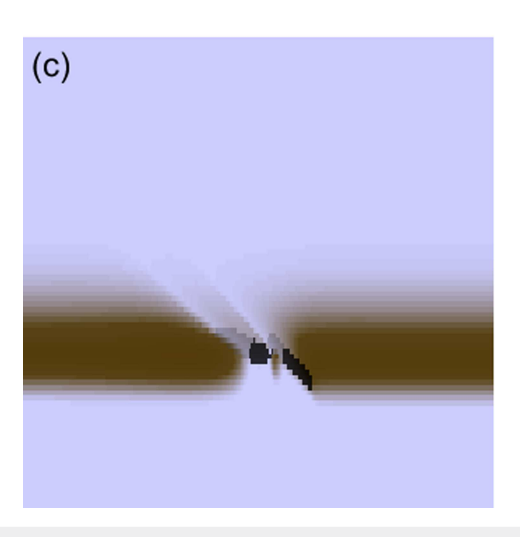
**FIG. 6.** (a) Angle of depression of wave propagation of a lead wave measured in the gel slice experiments as a function of  $[OH^-]$ , with  $[Al^{3+}] = 0.32M$ , blue line and  $[Al^{3+}]$  with  $[OH^-] = 2.5M$ , red line. (b) Angle of depression of wave propagation measured in simulations as a function of b with a = 7.5, blue line, and a with b = 55.0, red line. (c) Time average of the spatially averaged ratio [A]/[B] in the vicinity of the wave tip. Inset: Moving average of ratio vs time for a = 6.5, red line, a = 8.0, orange line, and a = 9.0, blue line, with b = 55. The spatial average of [A]/[B] is calculated at a given time step over a region of cells (i,j) ahead of the wave tip with  $i = x_{iip} + 2$  and  $y_{tip} - 2 \le j \le y_{tip} + 2$ .  $x_{tip}$  and  $y_{tip}$  are the current coordinates of the wave tip. (d) Measured propagation angle vs ratio for various initial values of [A] and [B].

This understanding allows us to more precisely identify the wave tip region, Fig. 5(d). In this region,  $P_2$  is either still increasing or is already above the critical value for templating. As such, cells on the edge of this region have the potential for new growth into empty adjacent cells. Growth upwards dies out quickly as this growth is into a region of higher concentration of outer electrolyte, which rapidly consumes  $P_2$ . The inhibited growth in this direction leads to thickening of the  $P_2$  structure. It is the relative rates of horizontal (forwards) and downward growth in the vicinity of the tip that determines the

overall direction of growth of the structure. Horizontal growth has a high propensity as the large concentration gradients of the inner and outer electrolytes, due to the presence of the structure, meet at the tip. This results in significant diffusive fluxes of both A and B, producing the necessary critical amount of sol for horizontal growth of  $P_2$ , Fig. 5. Downward growth also occurs, but less frequently, when the sol concentration is high enough below the wave tip. Since sol arrives primarily via the reaction of the inner and outer electrolytes, B must encroach around the tip to allow the buildup of C to the







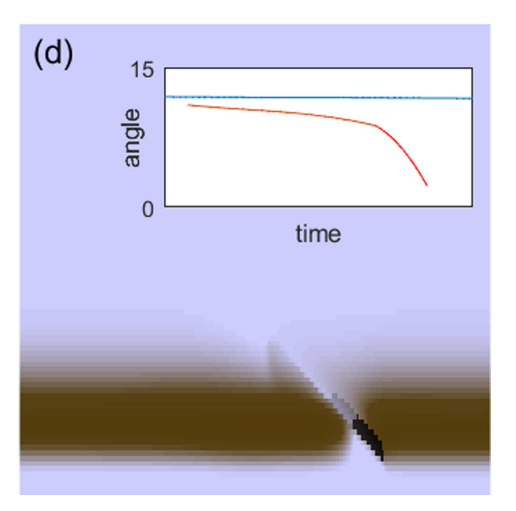


FIG. 7. Simulation of two waves merging at times (a) 85 000, (b) 140 000, (c) 165 000, and (d) 210 000 (a) Inset: trajectory of the lead wave tip, blue, and trailing wave tip, red. (d) Inset: Depression angle of wave propagation vs time for lead wave, blue, and trailing wave, red.

critical level. However, the concentration of the outer electrolyte is very low below the wave tip due to the removal of B through reaction with excess A at the tip. In the simulation shown in Fig. 5, [B] decreases by a factor of 5 along its upper perimeter. It then decreases by a further factor of 5 on the immediate underside of the tip. Anything that increases the penetration of B into the region beneath the tip will lead to, on average, tip propagation occurring at a steeper angle.

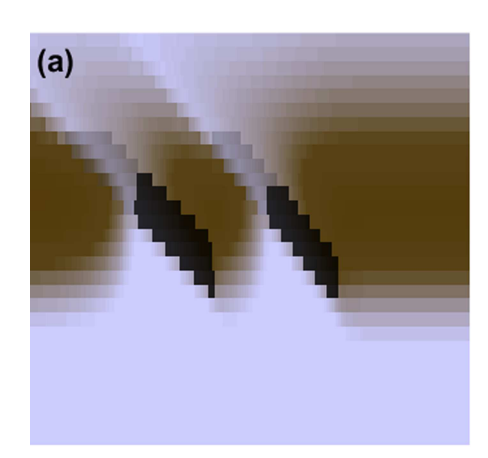
In the wave middle, Fig. 5(a),  $P_2$  is decreasing, owing to the reaction with the outer electrolyte. However,  $P_2$  is still large enough to prevent diffusion of the outer and inner electrolytes across the region. The wave back is identified as the point where  $P_2$  drops below the critical concentration that allows diffusion of A and B to recommence. This leads to the rapid formation of C and the resultant reattachment of the precipitation band, Fig. 5(a). The  $P_2$ 

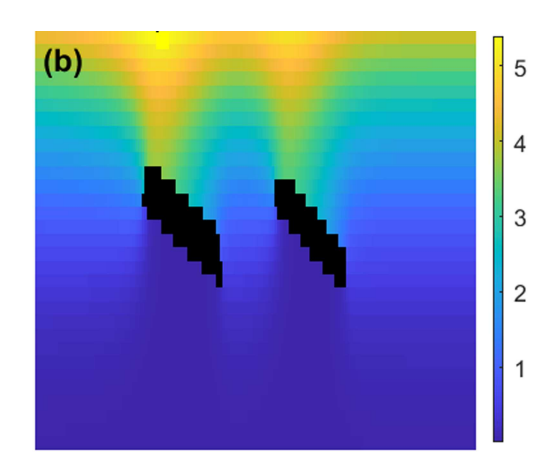
itself continues to slowly react with the outer electrolyte producing a slowly fading wave tail.

## A. Wave propagation angle

The changes in the wave propagation angle during wave merging can be used as the basis for developing a mechanism of the phenomenon. To achieve this, it is necessary to understand the factors that influence the wave angle and the wave properties that depend upon the wave angle.

For a given set of experimental initial conditions, a lead wave travels at an approximately constant angle, Fig. 4(a). This angle is found to depend on the initial concentrations used in an experiment, Fig. 6(a). The angle decreases as [Al<sup>3+</sup>] increases or [OH<sup>-</sup>] decreases. The angle of propagation is significantly more sensitive





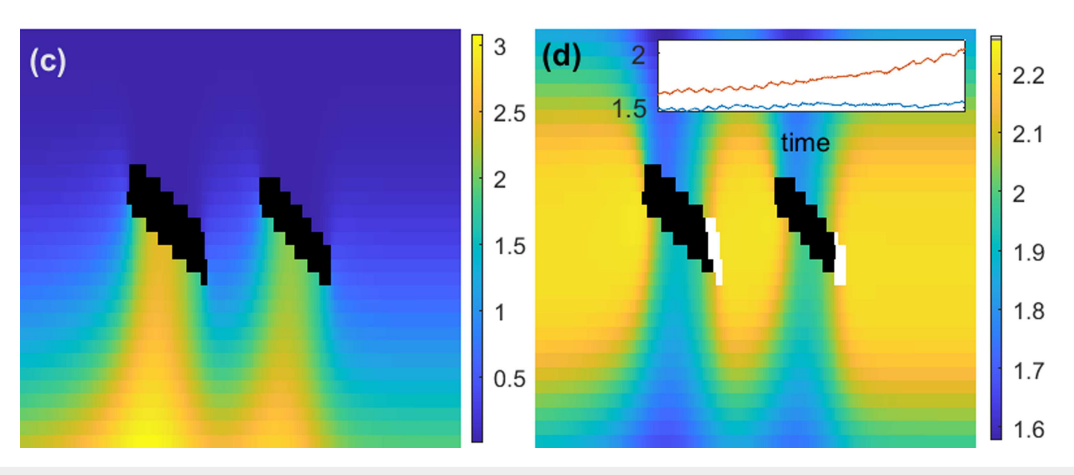


**FIG. 8.** Species distributions near a pair of merging waves. (a)  $P_2$  structure embedded within the precipitation band composed of  $P_1$  (brown). (b) Outer electrolyte concentration. (c) Inner electrolyte (d) Sol concentration. Inset: [A]/[B] ratio vs time for lead wave, blue, and trailing wave, red. Other details as in Fig. 5.

to changes in the inner electrolyte concentration, [Al<sup>3+</sup>]. Varying initial concentrations, and hence wave angle, also results in changes in the wave's horizontal velocity and the wavelength. The velocity increases and the wavelength decreases as the wave angle decreases (see the supplementary material).

Similar angular dependencies on initial concentrations are shown in Fig. 6(b) for the simulations, where larger initial outer electrolyte concentrations or smaller inner electrolyte concentrations lead to an increase in the wave angle. As in the experimental system, the simulations are more sensitive to changes in the initial inner electrolyte concentration. The variation in the wave tip's horizontal velocity with the wave angle also follows the same trends as in the experimental system. However, the variation in wavelength is not reproduced, with the simulation wavelength being approximately the same for different initial conditions.

At the start of Sec. VI, it was noted that we expect that increasing the encroachment of the outer electrolyte below the wave tip will lead to a steepening of the wave angle. This is in agreement with

the trends seen in the angular dependence on initial conditions. For example, for a larger initial outer electrolyte concentration, at a fixed initial inner electrolyte concentration, we expect that at an arbitrary depth and time the outer electrolyte's concentration will be relatively higher. Therefore, in the vicinity of the tip, we expect the outer electrolyte to be present, allowing more encroachment into the region below the tip.

To explore this understanding, we examine the ratio of the two electrolytes, [A]/[B], in the vicinity of the wave tip for different initial concentrations. Figure 6(c) shows that for a given set of initial conditions, this ratio, along with the wave angle, remains approximately constant. The value, however, increases as the initial concentration of the inner electrolyte increases or the initial outer electrolyte concentration decreases, Fig. 6(c). As with the propagation angle, the ratio is significantly more sensitive to changes in the inner electrolyte concentration. Since it is highly correlated with the wave angle, Fig. 6(d), it can be understood as a key ratio that influences the wave angle.

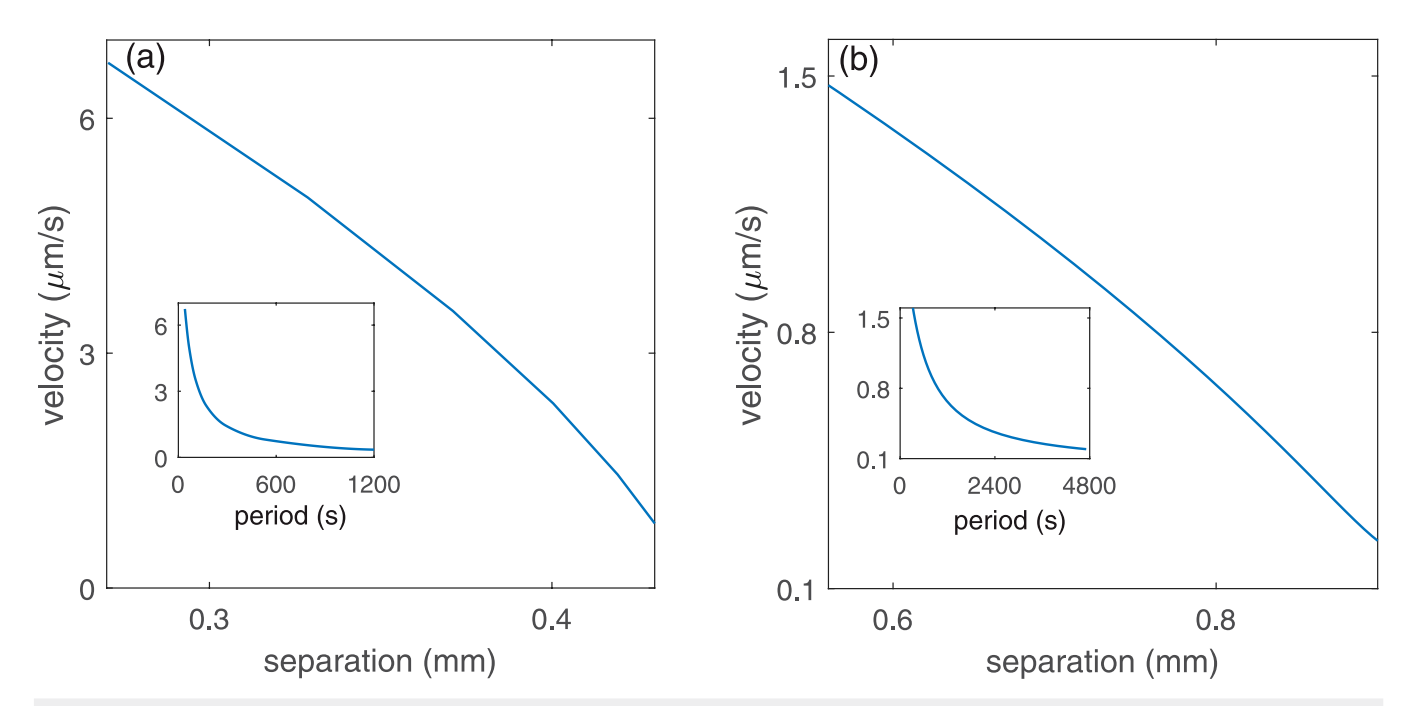


FIG. 9. (a) Dispersion relations using the relative wave velocity from (a) gel disk experiments and (b) gel slice experiments. The velocity is determined by fitting a nonlinear curve to the horizontal separation of the lead wave and its trailing wave, and then determining the gradient at each time. The separation at a given time is then plotted against the velocity at that time. For the gel slice experiments, the velocity is based on the separation of the wave backs. Insets: Velocity vs period. The period is determined by calculating the time it would take a wave moving at the relative velocity to travel the separation distance of the lead and trailing wave. The difference in length scales of the slice vs disk experiments arises because of the time at which we observe the behavior. In the gel disk experiments, the gel is not as deep, so we monitor the gel disk experiment earlier (relative to the gel slice experiments) when the velocity of the wave is larger and the wavelength of the waves is smaller.

## VII. WAVE MERGING

A wave observed traveling within the precipitation band consists of a diagonal structure that is continuously growing at the front and dissolving at the back. For a lead wave, the competing reaction-diffusion processes give an angle of growth of this structure that is approximately constant. The angle is dependent on the initial concentrations of inner and outer electrolytes.

In contrast, a wave traveling close to the back of a previous wave has a tendency to catch up with the lead wave and merge with it, as shown in the experimental results, Fig. 3. This process can be understood to occur due to changes in the angle of propagation of the trailing wave and associated changes in its tip's horizontal velocity and wavelength. A decrease in the propagation angle of the trailing wave as it approaches the lead wave is also seen in the simulations, Fig. 7. This decrease in angle is accompanied by an increase in the wave tip's horizontal velocity until eventually the trailing wave collides with the back of the lead wave and is annihilated. The changes in the wavelength prior to the collision, Fig. 4, are not reproduced in the simulations.

The difference in angles of propagation, between the lead and trailing waves, can be understood by considering the spatial concentration distributions of A and B that the trailing wave propagates into compared to the distributions that the lead wave propagates into. The presence of the lead wave results in a buildup of both A and B in its wake, Figs. B and B co. Since the buildup of A is deeper

within the gel, compared to that of B, we expect the ratio of [A]/[B] ahead of the trailing wave tip to increase and its propagation angle to shallow. The ratios for the two waves as functions of time are shown in Fig. 8(d). The closer the trailing wave gets to the lead wave, the larger the ratio, and hence, the more shallow the angle we expect, Fig. 6(d).

## VIII. DISCUSSION

Other studies involving wave merging in excitable systems have characterized the behavior in terms of the system's underlying dispersion relationship. 10,20 We can construct such a dispersion relationship using both the gel disk and the gel slice experimental data. In the case of the former, the velocity observed in the experiment corresponds to the horizontal component of a wave back's propagation. Analysis of the gel slice experiment shows that during a merging event, for the trailing wave, the wave tip's horizontal velocity increases and the wavelength decreases. The combination of these processes results in the wave tip of the trailing wave striking the wave back of the lead wave followed by the rapid merging of the wave backs of the two waves. An additional complication is that the back of the lead wave is also slowing down as the wavelength of a lead wave always increases with depth. This makes calculating a dispersion relationship for our system difficult since there are two velocities associated with the trailing wave, the wave tip, and

the wave back velocities, compounded by the changing wave back velocity of the lead wave.

To incorporate this complexity into the dispersion relationship, we can use the relative velocity of the waves. Figure 9(a) shows the relative velocity of the waves measured from the gel disk experiments vs the wave separation. An equivalent plot using the wave back separations, taken from the gel slice experiments, is shown in Fig. 9(b). Both plots show a characteristic negative slope, typically seen in systems showing anomalous dispersion, indicating an increasing velocity of the trailing wave as the wave separation decreases. Also shown in these plots is the dispersion relationship plotted using the wave period. Again, there is a characteristic negative slope with a sharp change in gradient as the period gets smaller. Similar behavior has been observed in other reaction diffusion systems. 10,20

The origin of these dispersion relationships can be understood in terms of the changes in the angle of propagation of the trailing wave during the merging event. Our studies of wave properties vs initial conditions show that both the wavelength and the wave tip's horizontal velocity depend on the propagation angle (see the supplementary material). Decreasing the wave angle results in the trailing wave tip moving faster than the lead wave tip and the trailing wave decreasing in length. The relative velocity of the wave backs seen in the dispersion relationship then follows from (1) the wave back of the trailing wave is moving faster than its wave tip since its wavelength is decreasing and (2) the wave back of the lead wave is moving slower than its wave tip. Note that the wavelength of the lead wave increases with depth.

We can next develop an understanding of the processes that lead to the changes in the propagation angle. Our simulations show that the propagation angle is dependent on the ratio [A]/[B] in the vicinity of the wave tip, Fig. 6(d). Smaller values of this ratio promote the production of sol below the tip increasing growth in the downward direction. The simulations also show that during wave merging the presence of the lead wave alters the concentration fields experienced by the second wave. This alteration is the result of the restricted diffusion of the reactants across the  $P_2$  structure and causes an increase of [A]/[B] ahead of the trailing wave. This ultimately leads to a shallower angle and resultant increase in tip velocity and decrease in wavelength. This mechanism is in contrast with anomalous dispersion seen in other excitation systems, which commonly requires the presence of a second inhibitor to provide a further feedback process.  $^{22,24}$ 

Our model qualitatively reproduces many aspects of the experimental system. These include the dependence of the propagation angle on the initial concentrations, the dependence of the wave tip's horizontal velocity on the propagation angle, and the decrease in the propagation angle of the trailing wave during merging. It also reproduces the dependence of the wavelength on the angle of propagation.

Our simulations fail to capture the dependence of the wavelength on the propagation angle. In the experimental system, the shortening of the wavelength as the wave propagation angle decreases is associated with the more rapid reattachment of the precipitation band to the wave back. A possible explanation for this is that the physicochemical properties of the  $P_2$  barrier are influenced by the concentration field it experiences during its formation.

At concentration gradients associated with shallower propagation angles, the  $P_2$  structure does not form as an effective barrier to hydroxide penetration and so reattachment occurs sooner. We do not expect that further refinement of the model incorporating such detail to impact our overall findings. The merging behavior is primarily driven by the concentration field in front of the trailing wave. It is unlikely that changes at the wave back of the trailing wave will strongly influence this upstream concentration field. We plan to investigate these processes further in future work.

Experimental observations suggest that the waves must be initially close enough to each other in order for waves to successfully catch up and merge within the timescale of an experiment. For example, in Fig. 2, we see wave 2 merges with wave 1 and wave 4 merges with wave 3. However, the resultant waves, 1 and 3, do not merge. Measurement of these waves indicates that there is a small decrease in their separation during the remainder of the experiment. Examination of Fig. 6 supports this observation, where wave 3 has a slightly smaller angle of propagation than wave 1.

The lack of a secondary merging event can be physically understood. When two waves have a large separation, the changes in the spatial distributions of A and B, due to passage wave 1, have time to dissipate. Wave 2 then experiences concentration fields very similar to that of wave 1 and so has nearly identical propagation properties. Our simulations indicate that, for a given simulation duration, there is a critical initial separation below which a trailing wave will catch up with a lead wave.

## SUPPLEMENTARY MATERIAL

See the <u>supplementary material</u> for movies of the top-view and side-view experiments and for further details of the numerical model used in this work.

## **ACKNOWLEDGMENTS**

This material is based on work supported by the National Science Foundation (NSF) (Grant No. CHE-2102137).

# AUTHOR DECLARATIONS Conflict of Interest

The authors have no conflicts to disclose.

## **Author Contributions**

Boshir Ahmed: Data curation (equal); Investigation (equal); Methodology (equal); Visualization (equal); Writing – review & editing (equal). David Mersing: Investigation (equal); Methodology (equal); Validation (equal); Writing – review & editing (equal). Mark R. Tinsley: Conceptualization (equal); Data curation (equal); Formal analysis (equal); Funding acquisition (equal); Investigation (equal); Methodology (equal); Project administration (equal); Software (equal); Supervision (equal); Validation (equal); Visualization (equal); Writing – original draft (equal); Writing – review & editing (equal). Kenneth Showalter: Conceptualization (equal); Funding acquisition (equal); Project administration (equal); Supervision (equal); Writing – review & editing (equal).

#### **DATA AVAILABILITY**

The data that support the findings of this study are available from the corresponding author upon reasonable request.

#### **REFERENCES**

- <sup>1</sup>R. Liesegang, "Ueber einige eigenschaften von gallerten," Naturwiss. Wochenschr. 11, 353 (1896).
- <sup>2</sup>A. Volford, F. Izsák, M. Ripszám, and I. Lagzi, "Pattern formation and self-organization in a simple precipitation system," Langmuir 23, 961
- <sup>3</sup>M. R. Tinsley, D. Collison, and K. Showalter, "Propagating precipitation waves: Experiments and modeling," J. Phys. Chem. A 117, 12719 (2013).
- <sup>4</sup>M. R. Tinsley, D. Collison, and K. Showalter, "Three-dimensional modeling of
- propagating precipitation waves," Chaos 25, 064306 (2015).

  5V. Nasreddine and R. Sultan, "Propagating fronts and chaotic dynamics in Co(OH)<sub>2</sub> Liesegang systems," J. Phys. Chem. A 103, 2934 (1999).
- <sup>6</sup>A. F. Taylor, "Mechanism and phenomenology of an oscillating chemical reaction," Prog. React. Kinet. Mech. 27, 247 (2002).
- <sup>7</sup>R. Field, E. Koros, and R. Noyes, "Oscillations in chemical systems. II. Thorough analysis of temporal oscillation in the bromate-cerium-malonic acid system," J. Am. Chem. Soc. 94, 8649 (1972).
- $^{\mathbf{8}}\text{P.}$  Hantz, J. Partridge, and G. Láng, "Ion-selective membranes involved in pattern-forming processes," J. Phys. Chem. B 108, 18135 (2004). <sup>9</sup>E. Nakouzi and O. Steinbock, "Self-organization in precipitation reactions far
- from the equilibrium," Sci. Adv. 2, e1601144 (2016).
- <sup>10</sup>N. Manz, S. C. Müller, and O. Steinbock, "Anomalous dispersion of chemical waves in a homogeneously catalyzed reaction system," J. Phys. Chem. A 104, 5895
- 11 I. Lagzi, "Controlling and engineering precipitation patterns," Langmuir 28, 3350 (2012).
- 12 M. Al-Ghoul, M. Ammar, and R. O. Al-Kaysi, "Band propagation, scaling laws and phase transition in a precipitate system. I: Experimental study," J. Phys. Chem. A 116, 4427 (2012).

- <sup>13</sup>A. A. Polezhaev and S. C. Müller, "Complexity of precipitation patterns: Comparison of simulation with experiment," Chaos 4, 631 (1994).
- 14S. C. Müller, S. Kai, and J. Ross, "Curiosities in periodic precipitation patterns," Science 216, 635 (2013).
- <sup>15</sup>S. C. Müller and J. Ross, "Spatial structure formation in precipitation reactions," J. Phys. Chem. A 107, 7997 (2003).
- <sup>16</sup>H. Nabika, M. Itatani, and I. Lagzi, "Pattern formation in precipitation reactions: The Liesegang phenomenon," Langmuir 36, 481 (2020).
- <sup>17</sup>M. Zrinyi, L. Galfi, and E. Smidroczki, "Direct observation of a crossover from heterogeneous traveling wave to Liesegang pattern formation," J. Phys. Chem. 95,
- <sup>18</sup>R. Sultan and S. Panjarian, "Propagating fronts in 2D Cr(OH)<sub>3</sub> precipitate
- systems in gelled media," Physica D 157, 241 (2001).

  19 M. M. Ayass, I. Lagzi, and M. Al-Ghoul, "Three-dimensional superdiffusive chemical waves in a precipitation system," Phys. Chem. Chem. Phys. 16, 24656
- <sup>20</sup>M. M. Ayass, I. Lagzi, and M. Al-Ghoul, "Targets, ripples and spirals in a precipitation system with anomalous dispersion," Phys. Chem. Chem. Phys. 17, 19806
- <sup>21</sup>I. R. Epstein and K. Showalter, "Nonlinear chemical dynamics: Oscillations, patterns, and chaos, J. Phys. Chem. 100, 13132 (1996).

  <sup>22</sup>N. Manz, C. Hamik, and O. Steinbock, "Tracking waves and vortex nucle-
- ation in excitable systems with anomalous dispersion," Phys. Rev. Lett. 92, 248301
- (2004).

  23 N. Manz, B. T. Ginn, and O. Steinbock, "Propagation failure dynamics of wave trains in excitable systems," Phys. Rev. E 73, 066218 (2006).
- <sup>24</sup>G. Bordyugov, N. Fischer, H. Engel, N. Manz, and O. Steinbock, "Anomalous dispersion in the Belousov-Zhabotinsky reaction: Experiments and modeling," Physica D 239, 766 (2010).
- <sup>25</sup>J. Christoph, M. Eiswirth, N. Hartmann, R. Imbihl, I. Kevrekidis, and M. Bär, "Anomalous dispersion and pulse interaction in an excitable surface reaction," Phys. Rev. Lett. 82, 1586 (1999).
- <sup>26</sup>J. Ross, S. C. Müller, and C. Vidal, "Chemical waves," Science 240, 460 (1988). 27S. Horvát and P. Hantz, "Pattern formation induced by ion-selective surfaces: Models and simulations," J. Chem. Phys. 123, 034707 (2005).